JOURNAL OF PROPULSION AND POWER
Vol. 24, No. 6, November–December 2008

Near-Surface Electrical Discharge in Supersonic Airflow: Properties and Flow Control

Sergey B. Leonov* and Dmitry A. Yarantsev†
Russian Academy of Sciences, 125412, Moscow, Russia

DOI: 10.2514/1.24585

The results of experimental and numerical investigations of the interaction between the near-wall electrical discharge and supersonic airflow in an aerodynamic channel with constant and variable cross sections are presented. Peculiar properties of the surface quasi-direct-current discharge generation in the flow are described. The mode with flow separation developing outside the discharge region is revealed as a specific feature of such a configuration. An interaction model is proposed on the basis of measurements and observations. A regime of gas-dynamic screening of a mechanical obstacle installed on the channel wall is studied. Variation of the main flow parameters caused by the surface discharge is quantified. The ability of the discharge to shift an oblique shock in an inlet is demonstrated experimentally. The influence of relaxation processes in nonequilibrium excited gas on the flow structure is analyzed. Comparison of the experimental data with the results of calculations based on the analytical model and on numerical simulations is presented.

Nomenclature

c_d	=	drag coefficient
c_p	=	specific heat at constant pressure
E	=	electric field strength
G	=	mass flow rate
H	=	total enthalpy of the flow
I, I_{pl}	=	electric current
M	=	Mach number of the flow
m	=	mass of gas
N	=	number density
P, P_{st}	=	static pressure in airflow
P_0	=	stagnation pressure in airflow
R	=	universal gas constant
R_b, R_{ba}, R_{bc}	=	electrical resistance in anode and cathode
Re	=	Reynolds number
T, T_r, T_v, T_e	=	gaseous, rotational, vibrational, and electron temperature
U, U_{pl}	=	voltage on discharge gap
V	=	velocity of flow
W, W_{pl}	=	power or power density
β	=	angle of oblique shock
γ	=	specific heat ratio
δ	=	boundary-layer thickness
ε_0	=	electrostatic constant
θ	=	angle of plasma wedge
μ	=	molecular weight
ρ_0	=	gas density in flow
τ	=	relaxation time

I. Introduction

RICH experience has been accumulated in using electrical discharges to control gas flows, and a wealth of data have been received in model experiments and by way of numerical calculations [1–10]. Several aerodynamic problems stimulate efforts in this field: drag-reduction, control of the inlet/diffuser performance, surface discharge effect on viscous friction, the improvement of the supersonic combustion efficiency, etc. An idea of the method can be formulated in the simplest manner as follows: modification of flowfield structure and, consequently, changing the pressure and shear stress near surfaces by means of bulk-force excitation in electromagnetic (EM) fields and heat release into predetermined locations with predetermined strength and spatial distribution of the parameters.

Three basic mechanisms of the discharge interaction with the flow are distinguished: thermal, magnetohydrodynamic (MHD), and electrohydrodynamic (EHD). This paper examines the conditions characterized by the flow parameters close to those in practical aerodynamics: that is, pressure $P = 0.1$–1 bar and velocity $M \leq 2$. The features of filamentary discharge behavior in the permanent magnetic field (MF) are described as well. (The EHD interaction seems to be negligibly small under these conditions.) It should be recognized that in such a situation, electrical discharges are, as a rule, essentially nonstationary and their spatial structure is highly heterogeneous. Filamentary plasma formations in various types of discharges can be seen beginning from the pressure $P = 30$ torr and higher. At pressures of over 100 torr, one can obtain homogeneous discharges only with the use of special methods. The diameter of such plasma formations depends on several parameters (on the amplitude of electrical current, mostly) and is usually 0.1–1 mm. The speed of their movement is close to the flow velocity.

Of special interest in the discussion of the flow structure transformation in channels is the generation of surface plasma, owing to its capacity to provide energy release and change the gas parameters in a predetermined zone of the flowfield, given the effective electronic control of the plasma location. It is almost an established rule that to appreciably alter the parameters of a high-velocity flow by means of a thermal mechanism, a large energy input (on the order of $W \approx 0.1 \times H$, where H is the total enthalpy of the flow in the corresponding stream tube) is required. However, in a number of important cases, the energy requirement becomes less stringent. For example, this is the case for the boundary layer. The plasma properties such as strongly inhomogeneous spatial structure, nonequilibrium composition, and nonstationary behavior allow reduction of the required energy to an acceptable level while still providing an adequate effect on the flow.

This paper considers only one type of interaction: namely, the effect of near-surface discharge between flush-mounted electrodes on the structure and parameters of supersonic airflow. The principal focus is on phenomena associated with plasma-induced flow

Received 12 April 2006; revision received 7 July 2008; accepted for publication 7 July 2008.

*Head of Laboratory, Joint Institute for High Temperature, Izhorskaya 13/19; Leonov@ihed.ras.ru. Associate Fellow AIAA.

†Ph.D. Student, Research Staff, Joint Institute for High Temperature, Izhorskaya Street 13/19.

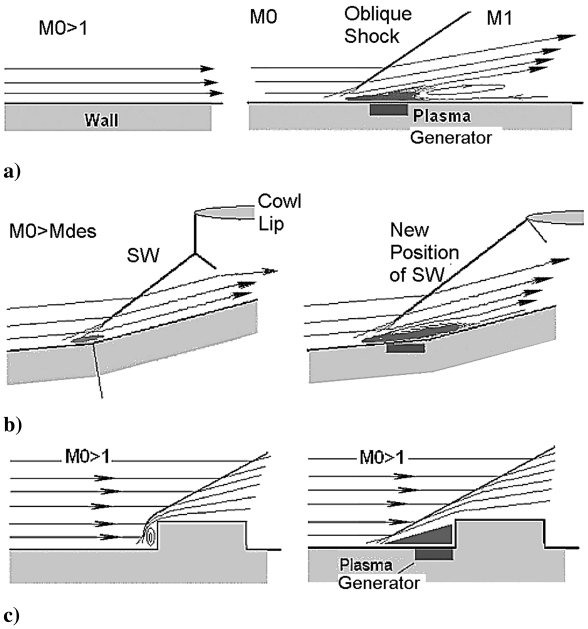

Fig. 1 Gas-dynamic configurations in which the effect of plasma-induced flow separation becomes apparent (SW indicates shock wave).

separation. Figure 1 schematically shows the principal types of aerodynamic situations in which the effect is important. The left images in Fig. 1 present undisturbed flow structure, and the corresponding right images depict the effects of flow modification. Supersonic flow control by near-surface discharge generation is illustrated in Fig. 1a. It can be applied in a number of cases (for instance, for stability control of supersonic combustor). Figure 1b demonstrates a typical configuration for super/hypersonic inlets. The shock position control can be accomplished by shifting the corner separation zone upstream. Another type of application is plasma control of the volume and parameters of already-existing separation zones at the backward-facing wall step, obstacle, and cavity. Figure 1c shows the effect of obstacle screening due to controlled development of a forward separation zone. Such separation control also affects the core flow in the channel, which was verified experimentally in the experiments discussed later in this paper. Numerous computational-fluid-dynamics (CFD)-based predictions, some data of model experiments, and a feasibility analysis of the flight experiment show that the use of electric discharge plasma is quite effective in several important aerodynamic (AD) situations. At the same time, it has to be noted that a local positive effect does not necessarily lead to desirable changes of flow structure in a whole system: the associated penalties should be taken into account as well.

II. Experimental Facility and Measurement Technique

The Joint Institute for High Temperature at the Russian Academy of Sciences PWT-10 and PWT-50 blowdown facilities have been developed for short-duration testing of electrical discharge behavior in supersonic and transonic flows. Figure 2 gives a simplified diagram of the PWT-10 facility. The gas-dynamic circuit has a high-pressure tank with a working pressure of 1–5 bar, a quick-action valve with an electromagnetic drive, an intermediate unit (plenum chamber), a supersonic nozzle at $M = 2$, a testing section, a diffuser, and a low-pressure container. Compressed air can be supplied along two parallel lines from tanks or a compressor. A key component of the facility is the quick-action valve with a cross section of around 20 cm^2 and electromagnetic control. The real time of the valve response and setting of flow is no more than 20 ms. A transient unit is needed to provide uniform profile of the gas velocity at the test section. The input section of the unit is 50 mm in diameter, and the rectangular output dimensions are 20×50 mm^2. The dielectric test section has a rectangular section measuring 20×50 mm^2. The vertical (long) walls are made of quartz glass. The horizontal walls

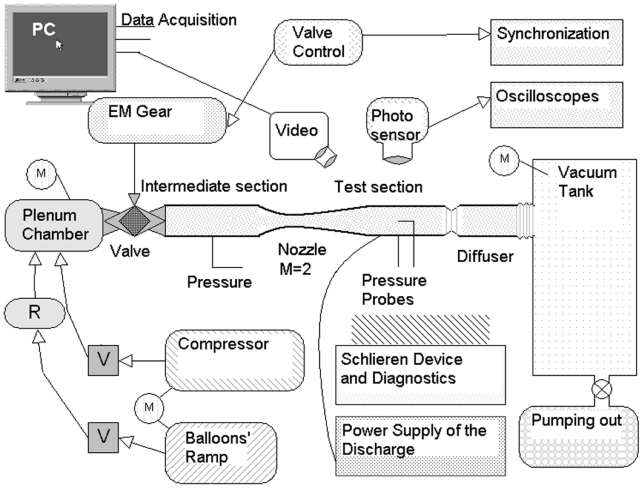

Fig. 2 Experimental facility PWT10/50 general layout.

are made of organic glass and have ceramic inserts. The test unit is 200 mm long. The vacuum chamber volume is 0.63 m^3. The facility PWT-50 has enhanced parameters at a cross section of 72×72 mm^2.

The experimental test bed provides the following characteristics of the flow: the Mach number $M = 1.8$–1.99, the static pressure $P_{st} = 100$–700 torr, the Reynolds number $Re = (4$–$10) \times 10^6 \times L$, the boundary-layer thickness in the testing zone is $\delta = 0.3$–0.5 mm, the typical gas flow rate through the channel is $G = 0.1$–0.6 kg/s, the duration of the quasi-stationary phase is 0.2–0.5 s, and the total enthalpy flow rate is $H \approx 20$–200 kW (from PWT-10 to PWT-50).

In the experiments outside the discharge region, an obstacle shaped as a contoured elliptical plate was mounted on a flat wall through the entire depth of the channel. The relative obstacle height was 10 or 17% (the measured values of the drag coefficient were $c_d \approx 0.2$ and 0.25, respectively). The models were mounted on a force balance, as shown in Fig. 3.

The PWT-10/50 facility test unit is furnished with a number of instruments; use is made of both standard and original methods of measurement and diagnostics of the gas and plasma conditions. Honeywell pressure transducers are used to monitor the mode. Time resolution of the transducers is not worse than 0.1 ms. Static pressure is measured in several points on the wall along the channel. The total pressure transducers are connected with pitot tubes that can be moved across the channel. Placed in the test section of the aerodynamic channel is an absolute pressure transducer for calibration of the system. The pressure profile is measured with the aid of an electronic commutator of pressure transducers for 32 measurement channels, connected to a PC through a PCMCI interface. The characteristic time of measurement is not worse than 0.3 ms for each channel. Figure 4 shows a diagram of the positioning of the main pressure transducers.

An original shadow (schlieren) device is used to record the flow structure with a possibility of high space and time resolution of images. A continuous illuminator, a ball flash lamp, or an IR laser diode were used as a light source. Some tests were conducted with the use of a surface-erosion discharge with a light flash of less than 1 μs duration. The images and shadowgraphs were recorded by a fast digital video camera Pulnix-6710 with an immediate processor control. A LOT-Oriel spectroscopic system was used to measure

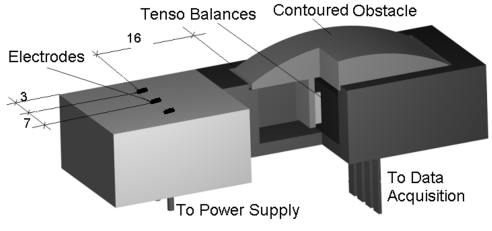

Fig. 3 Model arrangement in the test section.

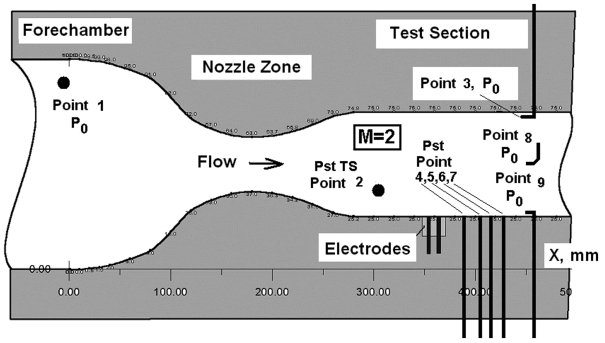

Fig. 4 Test-section arrangement.

plasma parameters. The plasma temperature was determined from the data of spectral measurements with the help of our original software for data processing. Use was made of standard and original electric current and voltage sensors, including a symmetrical divider, current shunts, and filters, with recording in Tektronix TDS-210 and HP-5062 digital oscilloscopes. The oscilloscopes were connected to a data acquisition system via the GPIB serial interface. The electric power release into the discharge was determined by calculation based on measurement of the discharge current-voltage characteristic. PSpice software was applied in calculations. The data were acquired by the system based on National Instruments hardware. The basic software was developed in the LabVIEW programming language. The synchronization system was built on the base of pulse generators and optical lines of data transmission to avoid electromagnetic noise.

III. Surface Electrical Discharge in Flow

A. Experimental Data

The electrodes for igniting surface discharges were flush-mounted with a ceramic insert wall. Power was supplied from a 5 kV constant voltage source through ballast resistors to all electrodes (there could be from 2 to 12 electrodes). Pulse step-up transformers were introduced to the circuit to effect breakdown under high pressure. Different connection diagrams were tested that, in the general case, were a superposition of longitudinal and transverse modes of the discharge with respect to the incident flow. These modes are shown in Fig. 5. Characteristic parameters of the discharge power supply are as follows: electrode spacing 5–15 mm, average current $I = 1$–10 A, voltage across the gap $U_{\text{pl}} = 150$–1200 V, reduced field $E/n = (10\text{–}100) \times 10^{-17}$ V · cm^2, and mean power deposition $W_{\text{pl}} = 0.3$–5 kW.

The longitudinal type of discharge in the conditions being described does not basically differ from a discharge in motionless gas. It features a distinct localization of plasma filaments and a relatively low voltage in the discharge gap ($U_{\text{pl}} = 150$–200 V), comparable with the value of the cathode drop. In contrast, high voltage is realized in the transverse discharge, which allows an effective input of energy to gas with a minimal number of electrodes. The results outlined next relate only to the discharge transverse mode in the three-electrode configuration (Fig. 5b).

Typical current and voltage oscillograms of the transverse discharge are shown in Fig. 6a. It is appropriate at this point to discuss some features of the transverse discharge. The oscillograms clearly show an appreciable level of noise in both the amplitude of voltage and discharge luminosity. This modulation is associated with the pattern of propagation of the transverse discharge in the flow. Basically, the discharge consists of plasma filaments moving with the flow downstream. At each instant of time, there is only one current channel (filament) between the pair of electrodes. The filament starts, then elongates, and finally breaks upon achievement of a certain length, at which moment the filament arises anew closer to the electrodes. In each such cycle, the voltage rises as the discharge channel grows in length, and the channel diameter increases, owing to thermal expansion. Thus, on average, the discharge is a thermal

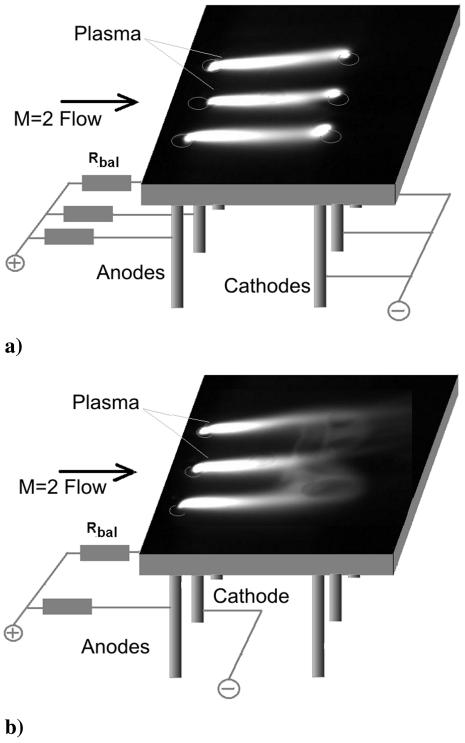

Fig. 5 Discharges appearance and wiring schematic: a) longitudinal and b) transversal.

wedge (discussed subsequently). At the instant of a new breakdown, there often occurs a light flash that is related to specific features of the power supply system. Figure 6b shows the correlation of voltage and luminosity that supports this mechanism. Figure 7 shows a diagram

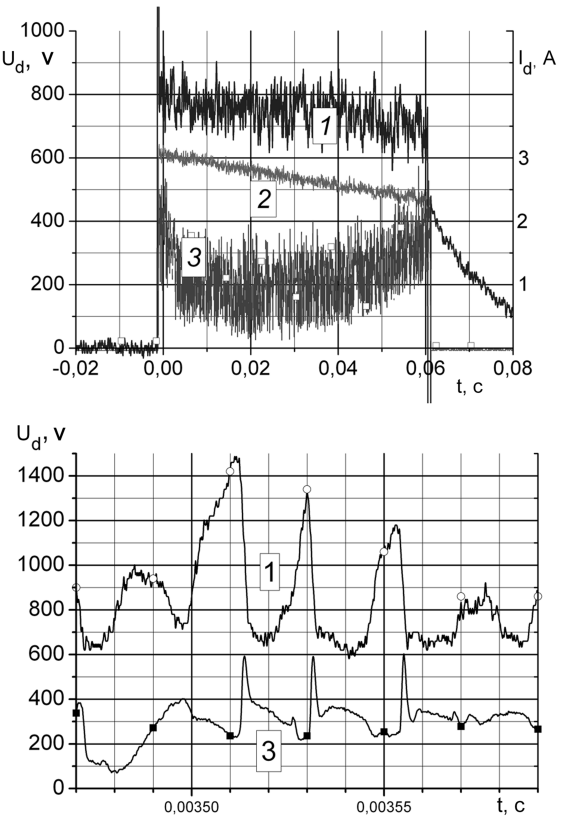

Fig. 6 Voltage-current oscillograms of transversal discharge in different time scales; 1 is the discharge voltage, 2 is the current through the anode, and 3 is the plasma luminosity.

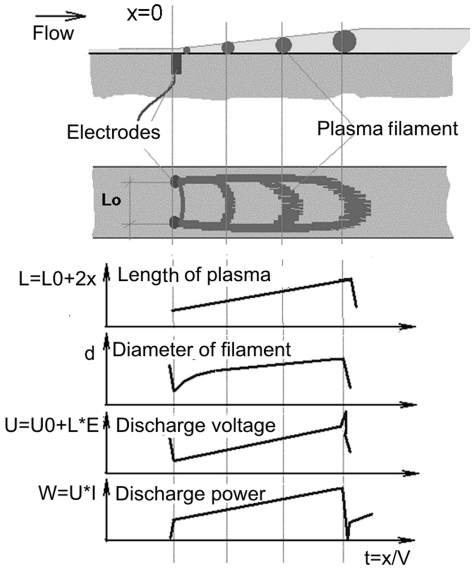

Fig. 7 Schematic of the relaxation mechanism.

of the relaxation mechanism of the transverse discharge. The frequency of relaxations depends mostly on the geometry of electrodes and the flow velocity and, to a lesser degree, on the power supply and pressure parameters. In our case, it ranged from 10 to 50 kHz. We call this type of discharge a *quasi-dc discharge*, meaning the essentially unsteady behavior of plasma filaments and oscillating voltage.

For a surface discharge, the velocity of the plasma channel motion may differ dramatically from that of the core flow, because the initial breakdown occurs in the boundary layer. The original method based on high-frequency modulation of the discharge current was used to visualize dynamics of the discharge channel in a transverse flow. A variable component with a 200 kHz frequency and amplitude of approximately 40% of the original value was added to the discharge direct current. Figure 8 gives the result of the discharge survey with a 30 μs exposure. The channel motion velocity turned out to be actually equal to that of an undisturbed flow (with a measurement error of around 10%, the rate of the discharge channel drift statistically accounts for about 90% of the flow velocity). In the case of a developed separately (discussed subsequently), however, the behavior of discharge filaments is more complex.

To measure the gas temperature in the discharge, optical spectra were recorded with the aid of a LOT-Oriel spectrograph with a charge-coupled device (CCD) camera, the spectral resolution of which is 0.04 nm/pixel, and the instrument function width is 0.12–0.15 nm. Thus, spectra with a partially resolved rotational structure were recorded in the experiment. In the standard case, the time window was 1 to 10 ms and the space resolution was around 5 mm. The spectra were measured in a pressure range from 100 to 350 torr with different discharge pulse durations. To measure the gas temperature in the discharge, use was made of a method for correlating the synthetic spectrum with the experimental one for the second positive system of nitrogen bands (transition 0-0) and the violet system of cyan bands upon addition of a small amount of CO_2. The values of rotational temperature for some regimes are given in Table 1. As will be clear from the data outlined subsequently, the

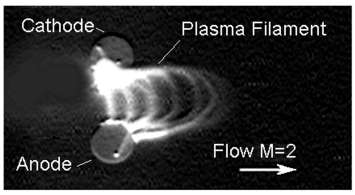

Fig. 8 Discharge image at discharge's current modulation of $f = 200$ kHz.

Table 1 Gas temperature T_r (kK) in discharge in dependence on conditions

Pressure, torr	Molecule	$I_{pl} = 0.8$ A	$I_{pl} = 2.3$ A	$I_{pl} = 4.3$ A
100	N_2	4.5 ± 0.5	5 ± 0.5	9 ± 1
100	CN	4.0 ± 0.5		8 ± 1
200	CN	3.0 ± 0.5		4.5 ± 0.5

measured temperature is somewhat higher than it follows from estimations based on power release. Normally, it is attributed to a considerable inhomogeneity of plasma parameters in the discharge region.

A possible explanation of the dramatic rise of gas temperature in the discharge as the power is increased is the following. The separated flow developing due to energy deposition begins to move upstream, sometimes farther than the electrode region [11,12]. As a result, the gas remains in the discharge region longer and is overheated.

For the main type of discharge power supply (quasi-stationary mode), the power deposition was calculated from the voltage measurement data in the discharge gap. Total power can be calculated by the following formula:

$$W_{pl} = U_{pl} \times (U_{ps} - U_{pl})/(R_{ba}/N_a + R_{bc}/N_c)$$

where W_{pl} is the power release to the plasma volume; U_{pl} is voltage in the plasma gap (root-mean-square value); U_{ps} is the power source voltage, N_a and N_c designate the numbers of anodes and cathodes, respectively; and R_{ba} and R_{bc} are ballast resistances in the anode and cathode circuit. In the case of an appreciable level of electric parameter modulation (which occurs, in particular, due to interaction of the discharge region with the flow), the voltage in the gap and the current are measured independently. In such a time scale ($t = 5$–20 μs), the plasma is not a linear load. Instantaneously supplied power is calculated by a simple formula: $W_{pl} = U_{pl} \times I_{pl}$, whereas the average supplied power is determined by means of an automatic integration procedure.

From the results of measurements, volt-ampere and watt-ampere characteristics of the discharge were built for different conditions. The discharge watt-ampere characteristics for the case in point are given in Fig. 9. The plot also shows the level of power deposition at which plasma-induced separation of the flow takes place (see the next section of the paper).

B. Model of Plasma-Layer Interaction with Airflow

The preceding features of the transverse surface discharge enable one to propose a simplified physical model. It has three basic assumptions:

1) The gas is weakly ionized, equilibrium, and ideal.

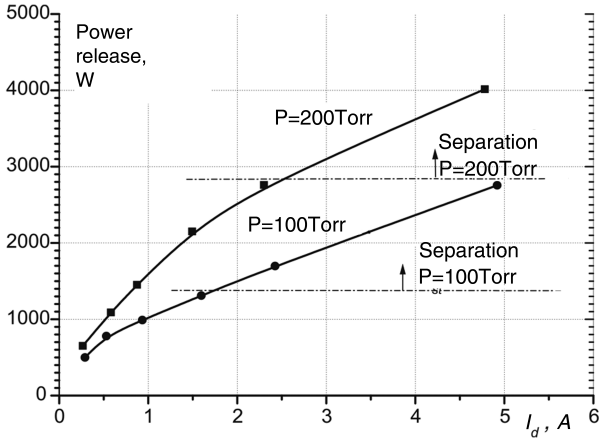

Fig. 9 Transversal surface discharge characteristics at two anodes, $M = 1.95$, interelectrodes gap 7 mm.

2) The discharge channel undergoes an isobaric expansion (2-D volume expansion).

3) The energy release is proportional to the discharge channel length.

At the final stage of analysis, the movement of an individual plasma channel is replaced by a continuous coordinate function (plasma wedge).

The energy deposition to the moving channel increases the gas temperature:

$$W = \frac{\partial m}{\partial t} c_p \Delta T = G1 \times \frac{R}{\mu} \times \frac{\gamma}{\gamma - 1} \times \Delta T$$

where W is the energy-deposition rate, m is the mass of gas in the channel, $G1$ is the average gas flow rate through the plasma layer, and ΔT is the gas temperature rise. The isobaric line condition gives the relation between the temperature variation and the filament volume:

$$\frac{m}{\mu} R \Delta T = p \Delta V$$

where $\Delta V = \pi/2 \times y \times \Delta y \times z$, and where y and z are the plasma-layer thickness and depth (filament diameter). A simple transformation provides the following expression for the plasma wedge angle θ:

$$\tan^2(\theta) = \left(\frac{\partial y}{\partial x}\right)^2 = \frac{\gamma - 1}{\gamma} \times \frac{2}{\pi \times z} \times \frac{1}{p \times V} \times \frac{W}{x}$$

where V is the flow velocity. To calculate the current value of W/x, one can use the relations between instantaneous and average power W_{av}:

$$W(x) = E \times I \times (L_0 + 2 \times x)$$

$$W_{\text{av}} = \frac{1}{\tau} \times \int_0^{x_{\max}} W(x) \frac{\partial x}{V}$$

where τ is the period of relaxations and L_0 is the electrode spacing. Hence, it follows that $W_{\text{av}} = W(x_{\max}/2)$, and the expression is simplified to

$$\tan^2\theta = \left(\frac{\partial y}{\partial x}\right)^2 = \frac{\gamma - 1}{\gamma} \times \frac{1}{\pi \times z} \times \frac{4}{x_{\max}} \times \frac{W_{\text{av}}}{p \times V}$$

Note that in the given notion, the plasma wedge angle does not depend on the initial thickness of the energy-deposition (input) zone y_0. In the context of the model, the gas temperature can be estimated as follows:

$$T_{\max} = T_{\text{st0}} \times \left(\frac{x_{\max}}{y_0}\right)^2 \times \tan^2\theta$$

Using typical values of the parameters (namely, $W_{\text{av}} = 1$ kW, $z = 20$ mm, $x_{\max} = 15$ mm, $V = 500$ m/s, $T_{\text{st0}} = 200$ K, $y_0 = y_{\text{bl}} = 1$ mm, and $P_{\text{st}} = 100$ torr) and the value of the specific heat ratio for $T = 3000$ K, one can estimate the expected angle of the plasma wedge and the average gas temperature at the end of the heating region: $\theta \approx 15$ deg and $T \approx 2950$ K.

Figure 10 gives a diagram of the plasma-layer interaction with the core flow. Assume that the plasma layer acts as a solid body so that the flow cannot penetrate it. This assumption is valid if a strong difference exists between the gas densities inside the layer and in the outer flow. In this case, the angle of an incident oblique shock β is uniquely related to the plasma wedge angle θ (see, for example, [13]): that is, to the level of deposited power W. In view of this approach, the flow turning angle and the pressure jump across the shock ΔP_{st} can be calculated. For small angles, the expressions are simplified:

$$\tan(\beta - \theta) = \frac{2 + (\gamma - 1) \times M^2 \sin^2\beta}{(\gamma + 1) \times M^2 \sin\beta \times \cos\beta} \approx \frac{1}{\sqrt{M^2 - 1}}$$

$$\Delta P_{\text{st}} \approx \tan(\theta) \times \frac{1}{\sqrt{M^2 - 1}} \times (\rho v^2)$$

As a result, we relate the structure and parameters of the flow with the level of power deposition in the surface discharge. The model certainly does not take many important features of interaction into account. However, this model allows one to make fairly accurate predictions of the surface discharge effect on the flow right up to the regime of thermal choking of the gas-dynamic channel. Given next is the comparison of experimental findings with the results of estimations with the model.

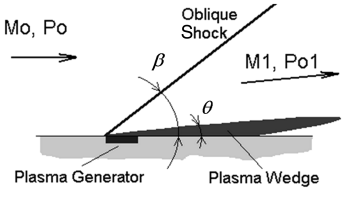

Fig. 10 Scheme of plasma–flow interaction.

C. Postdischarge Extrusive-Layer Thickness

The mechanisms of the plasma effect on flow cannot be reduced to the heating solely: they also appear in nonequilibrium excitation and volumetric forces generation in electromagnetic fields (electrostatic due to charge separation and magnetic due to the ampere's force). If the nonequilibrium excitation of the gas takes place, the area of power deposition does not equal the area of temperature increase. Such a discrepancy is important when a typical gas-dynamic time $t_{\text{gd}} = x/V$ is comparable with or less than a relaxation time. In other words, the length of relaxation may be comparable with the size of a streamlined object. A few types of excitation can be listed, but in the dense air, the vibrational excitation of nitrogen seems to be the most important. Figure 11 gives an estimation of the gas-temperature-dependent vibrational-translational relaxation length in supersonic flow. It is calculated on the basis of the data of [14]. It can be seen that in high-speed flow such a length can have meters of amplitude. Among others, two practical effects may be expected. As a rule, the result of heat release associated with plasma generation impedes the effect of MHD or EHD interaction. If the plasma is nonequilibrium, temperature is enough low, and velocity is high, the area of heat deposition occurs downstream of the interaction zone. The second consequence concerns the shape of the extrusive layer downstream of the plasma location: the expansion can be realized due to vibrational–translational (VT) relaxation instead of narrowing due to cooling. It is clear that a secondary expansion occurs, owing to some thinning of the primary plasma wedge.

The X profile of the extrusive layer located downstream zone of the electrical discharge location is critically important for analysis of consequences in terms of flow structure modification. One example is related to the steering of the inlet's shock-wave configuration when oblique shocks are applied for regulations of initial flow compression. Local condensed heat release leads to local flow

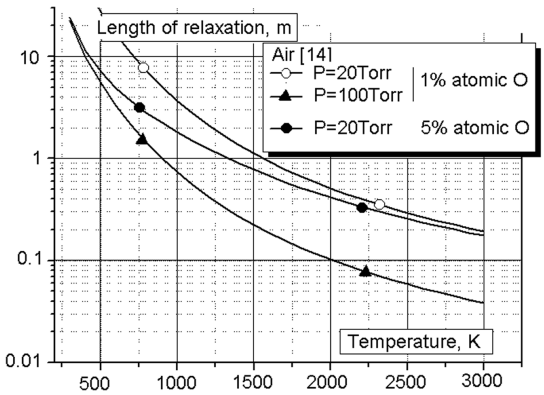

Fig. 11 Estimation of VT relaxation length at flow velocity $V = 500$ m/s.

modification as well. The idea of extrusive-layer lengthening due to protracted VT relaxation is quite promising to solve the problem.

An estimation of the extrusive-layer profile was fulfilled [15] considering a planar inviscid flow along a plane surface with electrical discharge burning transversely to the flow direction. The discharge-region length in the flow direction, l_d, and discharge thickness above the surface, h_d, were denoted as parameters. Specific discharge power $W = jE$ is distributed between vibrational and electronic excitation of molecules and direct gas heating; the corresponding parts of discharge power are denoted as η_v, η^*, and $1\text{-}\eta_v\text{-}\eta^*$, respectively. The energy stored in vibrationally and electronically excited states of molecules transfers into heat during τ_{VT} and τ^* time, respectively.

If the discharge-region length l_d in the flow direction is shorter than the vibrational–translational relaxation length $l_{\mathrm{VT}} = u_1\tau^*_{\mathrm{VT}}$, then the delayed energy extraction into the flow due to vibrational–translational relaxation has been shown to form an extrusion layer of thickness h near the surface [9,15]:

$$y(x) = h_d \exp\left[\alpha_W\left(1 - \exp\left(-\frac{x}{l_{VT}}\right)\right)\right]$$

where

$$\alpha_W = \frac{(\gamma - 1)\eta_V l_d W}{u_1 a_1^2 \rho_1}$$

is the relative vibrational energy stored in the flow due to discharge; x is the distance from discharge location; and u_1, a_1, and ρ_1 are the velocity, speed of sound, and density of oncoming flow. Relative layer thickness y/h_d versus relative distance x/l_{VT} is shown in Fig. 12 for different α_w values. As shown in [15], to obtain a notable expansion of the extrusive layer, the discharge power should be high enough to satisfy the condition $\alpha_W > 1$, which is correct for most lab-scale tests and in a wide range of flight situations.

D. Effect of External MF on Effectiveness of Plasma–Flow Interaction

The experimental data on improvement of the plasma–flow interaction effect by an external magnetic field were published in [6,9,11]. Here, we are focused on the features of filamentary transversal discharge behavior in both flow and external MF.

The dynamics of plasma filament in the flow with and without external MF was explored using a high-speed CCD camera and line-scan camera. A permanent magnetic field with a magnitude of up to $B = 1.2$ T is directed perpendicular to the surface, as shown in Fig. 13. The electrical current direction can be changed to obtain the assigned direction of magnetic force. The line-scan camera is adjusted on the axial line between electrodes along the flow. Stagnation/static pressure distribution and volt-ampere characteristics were acquired during the test.

The static pressure was $P_{\mathrm{st}} = 720$–100 torr at an initial Mach number value of $M = 0.2$–2. The quasi-dc discharge was generated in transversal mode. The electrodes were flush-mounted on the top and bottom walls of the duct, just near the surface. The electric power input to plasma volume was $W = 3$–10 kW for an interelectrode

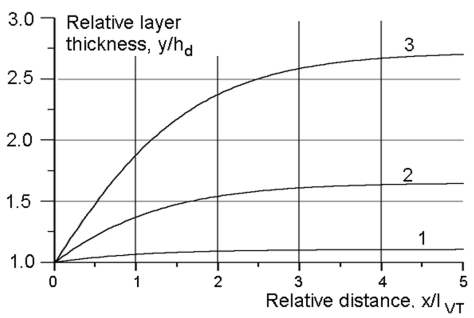

Fig. 12 Relative layer thickness y/h_d versus relative distance x/l_{VT} for various α_w values: 1 is 0.1, 2 is 0.5, and 3 is 1.0.

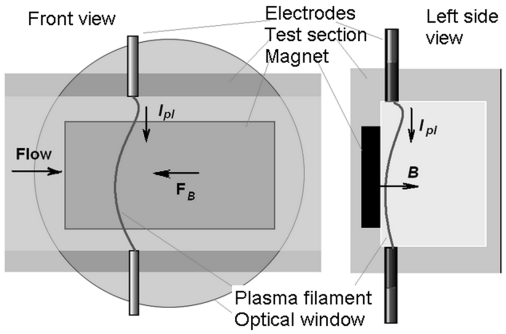

Fig. 13 Experimental scheme of test of plasma filament dynamics in flow and external MF.

distance of 50 mm. The typical electric current through an individual electrode was $I_d \approx 5$–50 A, and the duration of plasma pulse was $\tau = 20$–150 ms. The translational temperature of the gas was measured in discharge filaments using spectroscopic technique; the typical values were $T_g = 3.5$–6 kK, depending on experimental conditions. The increasing of power release leads to some rising of maximal temperature. The vibrational temperature weakly depends on power deposition, and in the case of moderate discharge power, it was higher than the translational temperature: $T_v \approx 8$–10 kK.

If the discharge is generated without MF, a standard relaxation mode takes place (see the preceding paragraph): plasma filament is blown down by the flow with velocity $V_{\mathrm{pl}} \approx 0.8$–$0.9$ V. The frequency of oscillations depends on the flow velocity and length of the plasma loop (that is a function of the power supply parameters). In the described case, it was $f = 5$–10 kHz. If the MF is applied for discharge generated in flow (the ampere's force F_m is directed ahead), the plasma filament motion is slowed down to complete stagnation (stop mode) or even a reverse direction of speed. In the stop mode, the translational temperature of the gas drops due to intensive cooling by the flowing through air, the length of the discharge filament decreases, the frequency of oscillations increases, and the reduced electric field rises up to $E/N = (5\text{–}7) \times 10^{-16}$ Vcm^2. Discharge plasma becomes more nonequilibrium with higher levels of vibrational excitation. This mode is favorable for generation of the extrusion layer, which has an expanding lengthwise profile. Samples of voltage-current record are shown in Fig. 14 without MF (pattern a) and in external MF (pattern b). It has to be noted that the averaged deposited power is almost the same for these regimes. In stop mode, the plasma filament affects the flow structure significantly.

Typical images of the discharge loops in two variants are shown in Figs. 15a and 15b. To realize a stop mode, the values of the main experimental parameters have to be in a distinct relation. The induced transversal plasma filament's velocity V_{ind} should be equal to the flow speed. The ampere forces $\boldsymbol{F_B}$ and gas-dynamic forces $\boldsymbol{F}_{\mathrm{gd}}$ might be equalized by current value and/or magnetic field strength adjustment. The conditions can be estimated roughly on the basis of the following consideration:

$$\boldsymbol{F}_B = [\boldsymbol{I}_{\mathrm{pl}} \times \boldsymbol{B}] \times L, \qquad F_{\mathrm{gd}} = c_d \times \rho/2 \times V_{\mathrm{ind}}^2 L d$$

$$F_B = F_{\mathrm{gd}}, \qquad V_{\mathrm{ind}} = V_0 \Rightarrow \rho \times c_d \times d \times V_0^2 \approx 2 I_{\mathrm{pl}} \times B$$

where d and c_d are the effective filament's diameter and effective drag coefficient of the plasma filament with attached mass. The diameter of the plasma channel is a complex function of density, temperature, current, and velocity of external flow. Practically, in ambient motionless air, the sound velocity of the plasma filament can be achieved at approximately $B = 0.1$–1 T and $I_{\mathrm{pl}} = 100$–1000 A.

The direct measurements of pressure distribution show that the discharge generation in MF significantly amplifies the effect of flow deceleration at conservation of the power deposition [16]. A subsonic area or separation zone is observed near the surface downstream the plasma place [6,7]. Oscillograms in Fig. 16 show the typical behavior of pitot pipe pressure downstream of the discharge

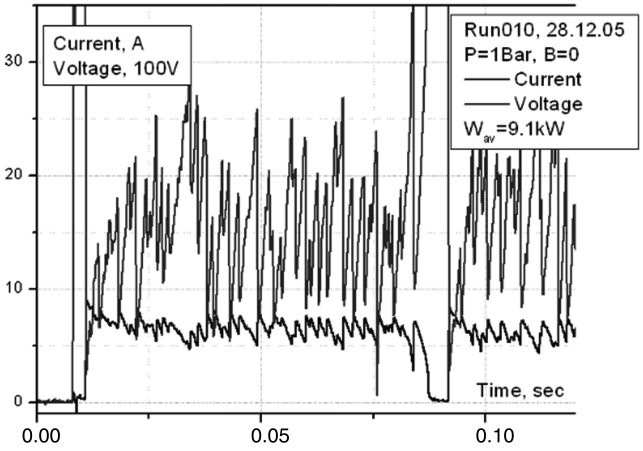

a)

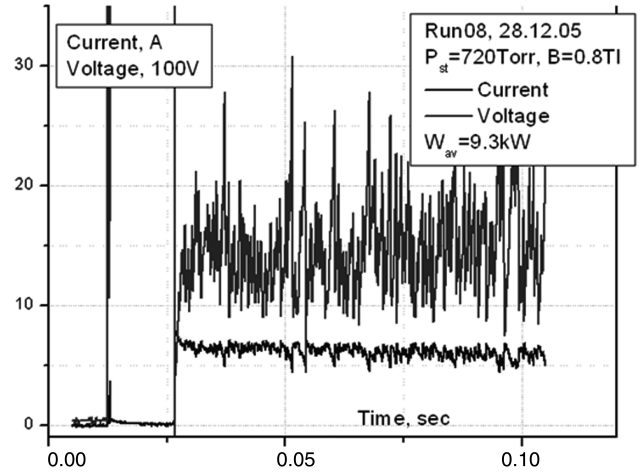

b)

Fig. 14 Volt-ampere records.

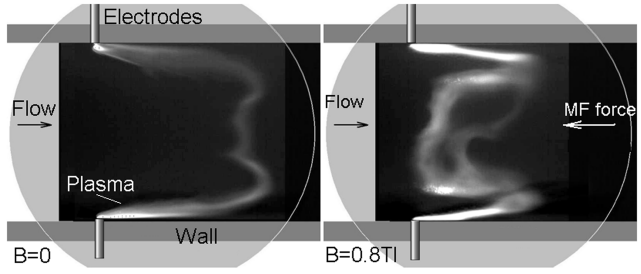

a) b)

Fig. 15 Plasma filament in flow.

zone. The mode with the current degradation was applied to recognize the features of interaction at different values of the ampere's force. The level of deposited power was approximately the same: $W_{pl} = 5$–7 kW, due to the voltage increases when the current drops.

In the second pattern, the mode with flow separation takes place when the amplitude of power deposition is rather far from the measured threshold for a freestream (see the preceding discussion). It means that the energetic efficiency of the flow stagnation in this case is significantly higher (note that the permanent magnets were used).

The fact of gas maximal temperature reduction is proved by spectral measurements. For example, the spectrum fragment is shown in Fig. 17. The presence of an N2+ band in the plasma spectra without MF is indirect evidence of a higher amplitude of temperature inside the plasma filament.

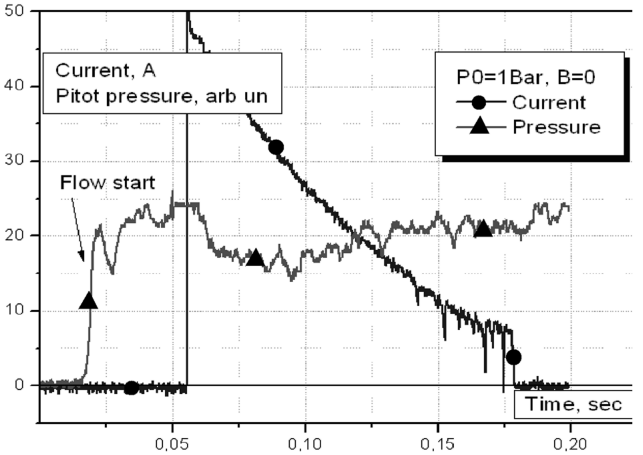

a)

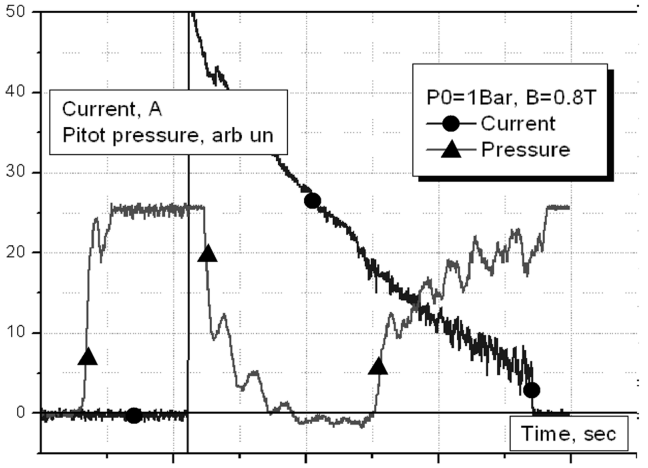

b)

Fig. 16 Current and pressure.

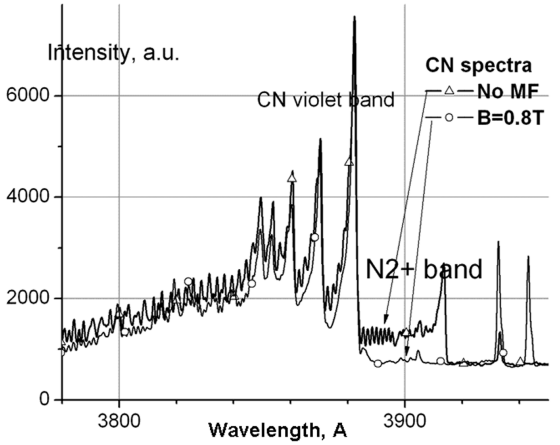

Fig. 17 Fragment of spectral measurements.

IV. Interaction of the Surface Discharge with the Flow (Experiment)

A. Artificial Separation of the Flow Near the Plane Wall

The generation of electrical discharge near the wall of the gas-dynamic channel brings about marked changes in the structure and parameters of supersonic flow. The air passing through the discharge region is heated and undergoes a number of plasma-chemical transformations; in particular, it is partially dissociated and ionized. This results in an intensive expansion of the plasma layer. The

pressure decreases downstream the energy-deposition region because of the cooling and recombination that may lead to the development of a zone of separated flow with posterior reattachment or without it. The flow structure is rather sensitive to variations of the power level in a particular range. Three basic patterns of flow were observed in the experiment. The result of the interaction depends on electrical power release in the discharge:

1) The heated layer is only produced near the surface, when the level of energy deposition is relatively low: $W < 1$ kW for $P_{st} = 100$ torr. The flow velocity downstream the electrodes may be lower or higher than the initial one. A concomitant oblique shock has a small amplitude and its angle is close to the Mach characteristic. The Mach number of the flow varies by less than 10%.

2) Local separation with reattachment and subsonic layer downstream is $W \approx 1$–1.5 kW at $P_{st} = 100$ torr. The Mach number of the main flow downstream of the oblique shock drops to $M = 1.42$–1.5.

3) The vast separation zone outgoing to the exhausting diffuser is $W > 2$ kW (10% of the flow enthalpy) at $P_{st} = 100$ torr. The visible amplitude of plasma-induced shock increases. The entire flow is transformed significantly. At the power increasing upward of 4 kW, the AD channel choking mode is realized.

Two basic methods were used to study the situation: the shadow (schlieren) method and measurement of pressure distribution. Figure 18 shows shadowgraphs of the flow without the discharge and upon interaction with the discharge for deposited power of $W_{pl} \approx 2.3$ kW at $P_{st} = 200$ torr. In the last case, there is a local separation with subsequent attachment. Unfortunately, the shadow patterns per se make it impossible to perform a detailed analysis of the flow structure in the plasma-layer zone. The analysis of pressure distribution is used for this purpose.

Figure 19 gives the records of temporal behavior of the pressure in different points of the gas-dynamic channel. To have an opportunity to look into the curves, most characteristic points of measurements are allowed to stand. Point a is pressure in the plenum chamber (it

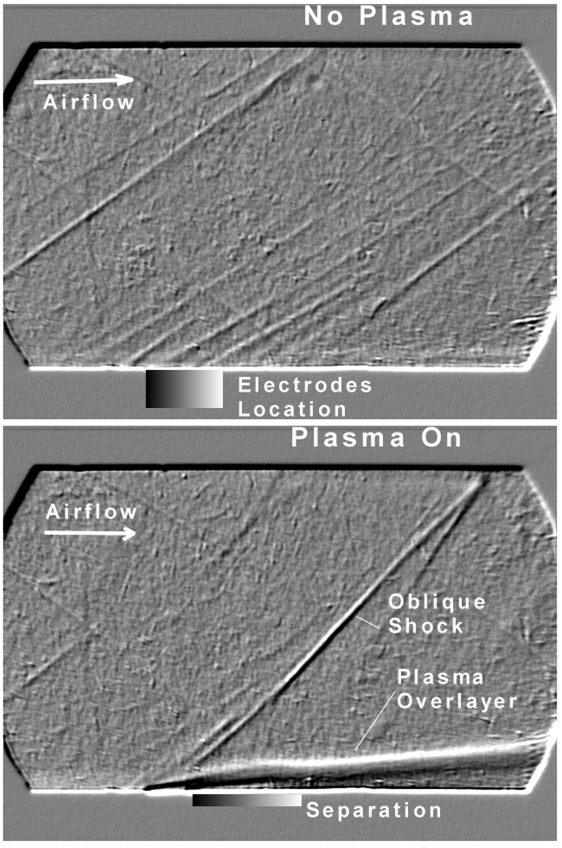

Fig. 18 Schlieren photographs of plasma–airflow interaction; discharge is off/on; and exposure is 30 μs.

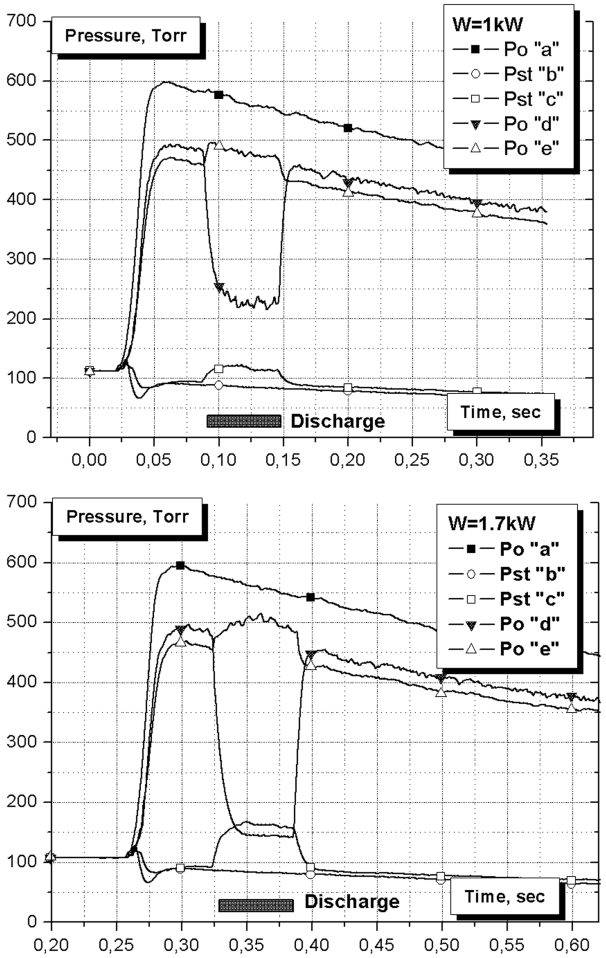

Fig. 19 Pressure redistribution at different power deposition.

slightly drops with time), point b is static pressure upstream the discharge area, point c is static pressure in the plasma-layer region 20 mm downstream, point d is readings of the total-pressure probe in the plasma layer 40 mm downstream, and point e is readings of the total-pressure probe on the channel axis 60 mm below the discharge region along the stream. The measurement data show that a situation is considered to be standard when the total-pressure-probe readings at the lower wall (where the discharge plate is mounted) appreciably decline and the static pressure in this region rises. In so doing, there is an essential difference in the cited cases. If with $W = 1$ kW a sonic flow with the Mach number $M \approx 1$ is realized in the wall region, then as the energy deposition further increases, the flow structure is transformed into a separated one with the formation of a circulation zone. This has an effect on the behavior of pressure in the wall region: the pressure due to the pitot tube becomes less than the static pressure; that is, the velocity vector is inverted. As the energy-deposition power increases, the main flow velocity varies gradually from $M = 1.98$ to 1.42, together with an increase of the oblique shock angle. Because of shock losses, stagnation pressure drops and is reflected in a certain growth of pressure in the pitot tube P'_o on the flow axis.

The formation of a vast circulation zone outside the energy-input region is of a threshold nature by the level of power. The experiments failed to register the mode of smooth transition from a subsonic flow at the wall to a separated one. Figure 9 shows an energy threshold of the formation of such configuration. It turned out to be proportional to the gas pressure in the conditions of the given experiment and equal to $W/P_{st} \approx 10 \times z$ W/torr, where z is the discharge-region depth. This is a rather high value, bearing in mind practical problems.

It is obvious that the discharge generation near the wall brings about a change of the flow in the whole gas-dynamic channel; in particular, the Mach number of the main flow decreases. An

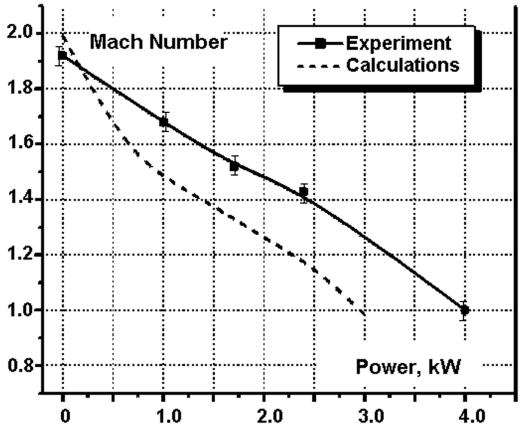

Fig. 20 Mach number dependence on power deposition in near-surface discharge.

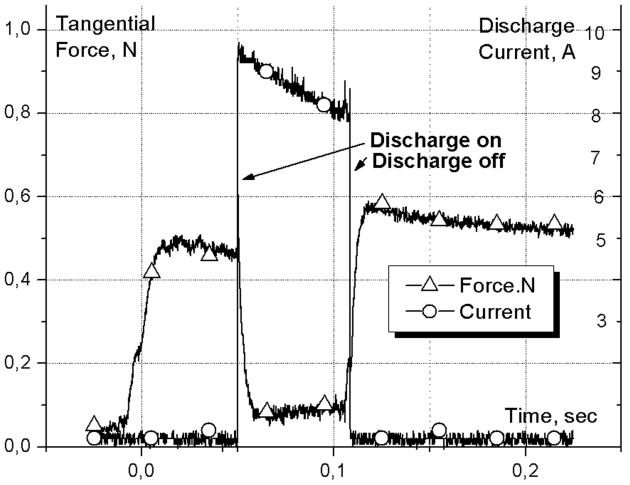

Fig. 21 Drag force reduction on surface obstacle under plasma generation.

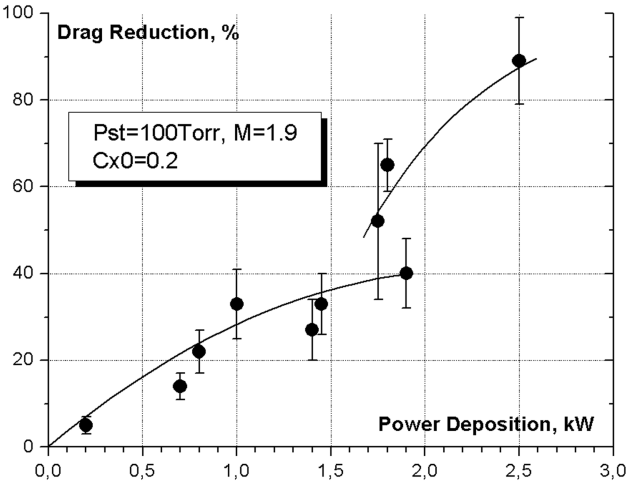

Fig. 22 Drag reduction vs input power to surface discharge.

appropriate dependence was derived experimentally for the point $x = 60$ mm and $y = 25$ mm: that is, in the channel axis downstream of the discharge region but upstream of the shock reflected from the upper wall. The result is shown in Fig. 20 for the initial Mach number $M = 2$ ($M = 1.96$ in the electrode-setting section) and pressure $P_{st} \approx 100$ torr. For comparison, the calculation result due to the preceding considered model is given as well. Because of the unaccounted dissipation of deposited power, the calculation yields values of the Mach number that are somewhat lower than the experimental values. Given next are the data on total pressure loss (see Table 2). It must be emphasized that the surface discharge does not give rise to additional turbulization of the flow.

Formation of the separation zone in and downstream of the energy-deposition region is not a trivial phenomenon. We made an attempt to numerically simulate the situation on the basis of the system of Navier–Stokes equations. The discharge was represented as an energy-deposition zone of different geometries. The numerical calculation described the flow structure and parameters adequately close to the experiment, right up to the values of gas temperature in the discharge region. However, it failed to show the effect of artificial separation due to the energy being deposited in the flow near the wall in the conditions of rather wide limits of parameter variations. It seems that further studies will make it possible to resolve the aforementioned contradiction.

B. Effect of Obstacle Screening on the Wall

Generation of a low-density near-wall layer of gas (and, more so, separation of the flow outside the discharge region) leads to an appreciable reduction of loads on the obstacle mounted on the wall downstream. The data on the reduction of drag of AD models, given subsonic and transonic streamlining, were published earlier (for example, in [3] and [12]). In this paper, the phenomenon of obstacle screening was investigated experimentally with the aid of a small contoured body with a drag coefficient $c_d \approx 0.2$ (see Fig. 3), arranged on a microbalance downstream of the discharge region at a distance of $x = 5a$, where a is the profile thickness. Figure 21 gives an example of measurement of the X-axis force upon operation of the discharge. A small zero drift is associated with an incomplete temperature compensation of the balance. One can readily see a significant decrease of the force (which, in some cases, accounted in 95% of the initial value). Figure 22 shows the drag-reduction effect as a function of the deposited power. Further increase of power causes thermal choking of the gas-dynamic channel. It is seen that the data can be conventionally divided into two groups by the level of effect. At $W_{pl} > 1.7$ kW, the size of the plasma-induced separation zone exceeds the obstacle thickness and the effect dramatically grows. Energetic efficiency of the obstacle drag reduction thereby does not exceed the 20% that, by the way, correlates with the previously made conclusion about low efficiency of the energy method to reduce c_d of streamlined bodies [17].

Table 2 Total pressure recovery factor P_02/P_0; $M_0 = 1.94$–1.98 and $M_2 = 1.42$–1.45

Power, kW	0	1	1.4	1.7	2.4	2.7
Solid wedge	0.77					
Plasma		0.86		0.8	0.81	0.8
Wedge + plasma		0.71	0.71		0.8	0.81

C. Control of Flow Parameters in the AD Duct

Generation of the surface discharge results in the variation of flow parameters in the preceding channel. In this part of the paper, we examine a gas-dynamic situation in which the flow in the AD channel is originally disturbed and there is a need to somewhat reduce loss in the channel (possibly for the time being). Similar cases are rather typical, for example, in solving a problem of starting up supersonic intakes and diffusers. In our case, the losses are modeled by putting an obstacle on the wall surface with a chord height of 17% at a distance $x = 3a$ from the discharge zone.

Typical shadowgraphs of the interaction are shown in Fig. 23 in the absence of discharge and in the case with it. The schlieren system was adjusted for visualization of oblique shocks incident from the bottom wall to the upper one. Following generally accepted notions about the value of losses in the supersonic channel, one can assume that they may be smaller in the second case because of the shock slope angle (calculated by the position of the reflection point from the upper wall) declined from 60 to almost 45 deg.

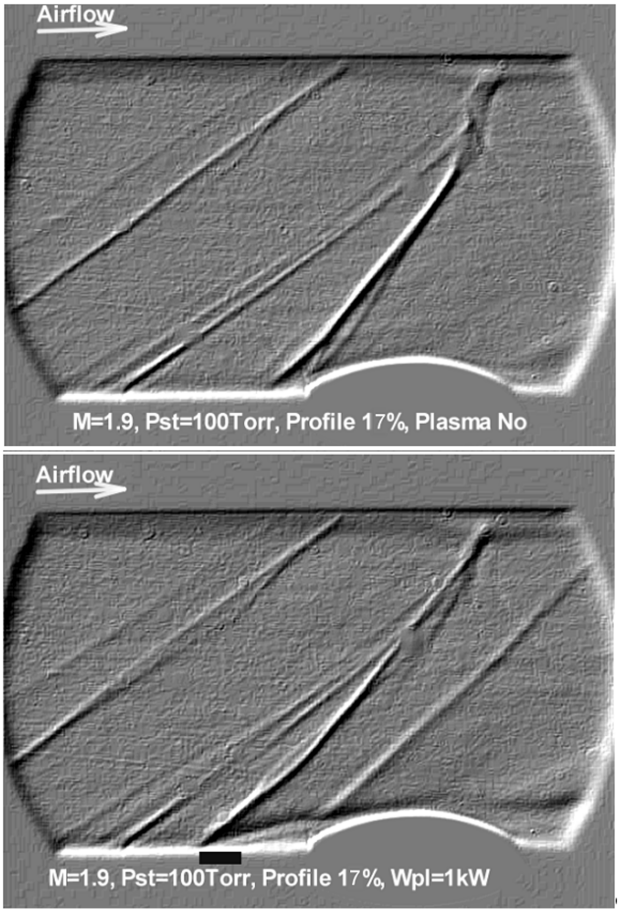

Fig. 23 Schlieren images of discharge effect at different power deposition.

The surface discharge has a greater effect on losses in the channel if the initial losses are significant due to mechanical reasons. This proposition is clearly demonstrated in Fig. 24, in which one can see the oblique shock angle β (see Fig. 10) as a function of the deposited-energy level for obstacles with a height of 10 and 17% in respect to the chord. It is also clear that with the power level higher than the threshold level for the generation of a developed separation, the position and amplitude of a shock are dictated only by the discharge parameters and do not depend on the obstacle height in certain limits. Also outlined here are experimental data for a discharge without an obstacle and the calculation by a simplified model. We notice that the calculation produces a correct trend. Given a higher power, the calculation yields greater values of the angles and lesser levels for the channel thermal choking that is associated with increasing of losses in the discharge. It is clear that there is a known arbitrariness in selecting the values of $x_{\max}$ and γ, yet the comparison points to a fairly good coincidence in reasonable limits of the parameters variation.

Despite an explicit improvement of the flow upon generation of the discharge upstream of a mechanical obstacle in the channel, a reply to the question about the overall pressure loss does not seem obvious, particularly in the development of unreattached flow. In experiments, the situation also becomes complicated by a relatively high level of viscous loss on the constant-section channel walls. Detailed measurements of pressure distribution in the channel were performed for three cases: namely, a solid wedge with the angle $\theta = 14$ deg and 20 mm long on the channel's bottom wall, a transversal surface discharge in the same place with the power $W_{\text{pl}} = 0$–3 kW, and the discharge upstream of the wedge at a distance of 16 mm. Measurements of the factor of the total pressure recovery relate to the point on the channel axis located downstream at a distance of 4 sizes of the channel on the vertical wall compared with the value in the section of arrangement of the wedge and electrodes. The initial Mach number of the flow was $M = 1.95$–1.98 at $P_{\text{st}} = 100$ torr in the measurement section $M2 = 1.42$–1.46. The results are shown in Table 2.

It is clear that beginning from a certain level of power, the pressure loss in the originally disturbed flow can be reduced to some extent. With the discharge generation upstream, the mechanical obstacle finds itself in the separation zone and a soft plasma wedge introduces less loss than with a solid body. On further increase of power, the pressure loss naturally grows, right up to thermal choking of the channel.

D. Flow Control in the Inlet's Configuration

We pose the results of this section as a demonstration of nonequilibrium plasma advantages to control of supersonic flow structure [9,15]. The experimental scheme is shown in Fig. 25 with the scheme of the model 3 shock-wave inlet. Oncoming flow in the duct with a height $Y_0 = 50$ mm has a Mach number $M = 2$ and static air pressure $P_{\text{st}} = 100$–300 torr. The measured translational gas temperature in the discharge zone is about $T_g = 3000$ K, and so the length of relaxation could be expected as a value of several centimeters (see Fig. 11). All electrodes were flush-mounted and do not affect the flow. To recognize the effects of VT relaxation, the experiments were fulfilled in air, argon (no VT excitation), and carbon dioxide (short time of VT relaxation).

Figures 26a, 26b, and 27 present the typical data of the model configuration test in air. The first photograph is the schlieren image of undisturbed flow structure. The second photograph shows the flow

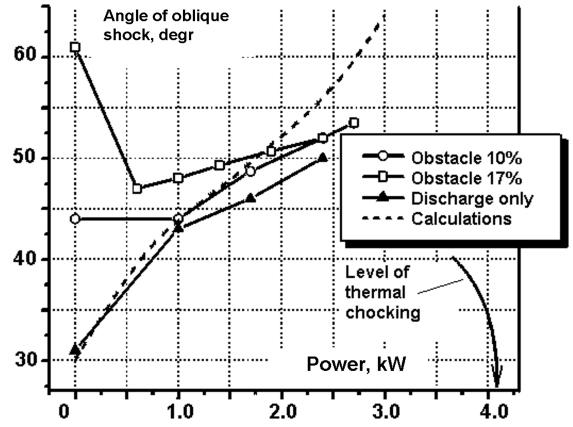

Fig. 24 Angle of oblique shock in duct with obstacle in dependence on power release at $M = 1.9$ and $P_{\text{st}} = 100$ torr.

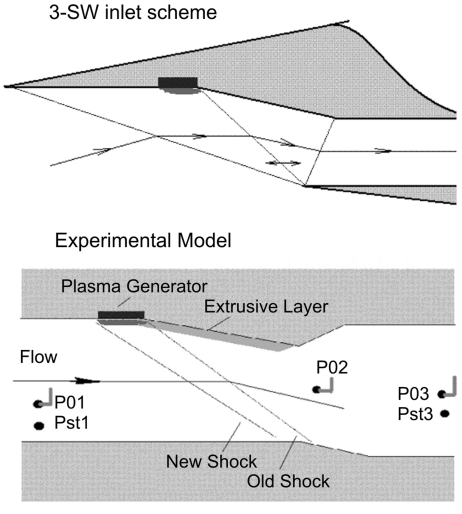

Fig. 25 Experimental scheme of quasi-dc discharge tests.

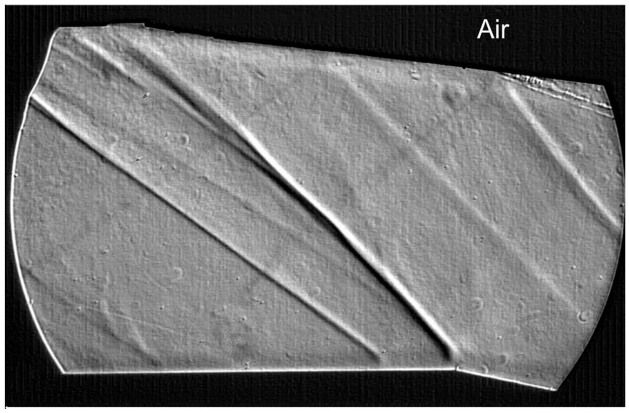

a)

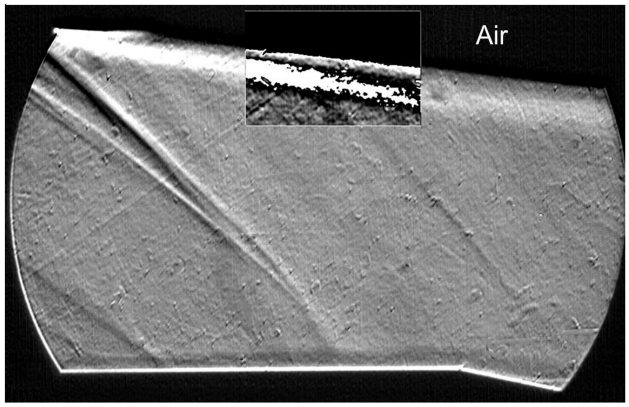

b)

Fig. 26 Schlieren photos: a) undisturbed flow and b) at the surface plasma generation in air.

structure when the plasma generator was switched on. The insertion allows recognizing the thickness of the extrusive layer on the wedge downstream of the plasma area (postplasma layer). Figure 27 presents data on pressure distribution measurements: $P_0 1$ is the stagnation pressure upstream (in the fore chamber), $P_0 2$ is the pressure from the pitot pipe at a distance 100 mm downstream of the plasma zone, $P_0 3$ is measured at the end of the duct (200 mm downstream), $P_{st} 1$ is the static pressure upstream of the interaction zone, and $P_{st} 3$ is the static pressure at the end of the duct.

The data obtained show that the surface discharge generated upstream of the wedge leads to a shifting of oblique shock upwards and to increasing of the shock angle. The extrusive-layer thickness rises up with the distance and reaches the magnitude $h_{pp} \approx 7$–9 mm 40–50 mm downstream of the plasma zone. Accordingly, the shock position on the opposite wall is shifted as well. Figure 27 shows that the stagnation pressure on the axis drops approximately by 8%, whereas the stagnation pressure downstream does not change. The decrease of static pressure $P_{st} 3$ means some reduction of pressure loss in a whole duct.

Similar tests were performed with argon and carbon dioxide as the working gases. Comparison of the results is presented in the Table 3, in which the shock's shift upstream is measured on the bottom wall, and the thickness of the extrusive layer (in millimeters) is measured 40 mm downstream of the electrode positions. In contrast with the air

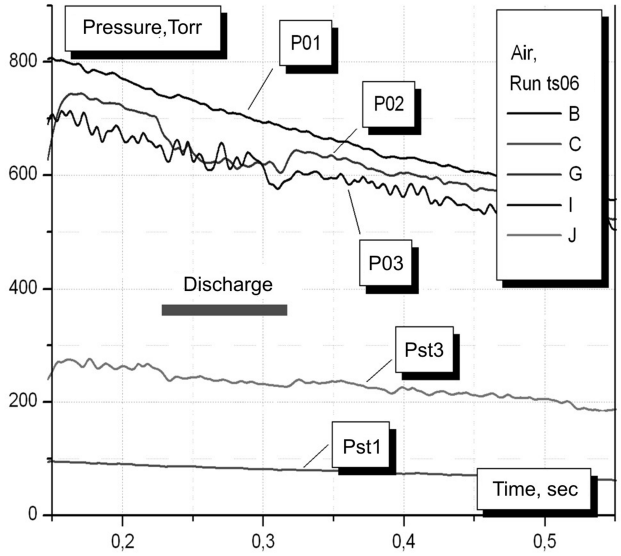

Fig. 27 Pressure distribution at the plasma generation in air.

test, some decrease of oblique shock angle is observed for argon and CO_2. The extrusive-layer thickness was in the range of $h_{pp} = 4$–5 mm, in spite of the fact that the specific power release was conserved at the same level. The result of surface plasma action in CO_2 is close to that in argon. In this case, a weak flow deceleration takes place without notable total pressure reduction. It should be noted that the flow regime in the whole duct has been modified weakly.

The comparison of longitudinal behavior of extrusive-layer thickness for these cases is shown in Fig. 28. It is measured by schlieren technique; that is, it is a thickness of density irregularity. The length of direct power release due to Joule heating is about 20–30 mm. Here, the difference in expansion can be explained by different thermodynamic properties of the gases: $\mathrm{d}h_{pp}/\mathrm{d}W \sim (\gamma - 1)/\gamma$. Below this line, three processes are in competition: cooling with some impaction, turbulent mixing, and extra expansion due to energy relaxation from the internal reservoir. It can be seen that the discharge in air demonstrates a favorable behavior to control of shock positions in duct-driven supersonic flow.

E. Flow Control Behind the Wall Step

The control of the flow behind the wall step and in the cavity of the supersonic duct is important for adjustment of the supersonic combustor possessed of such an arrangement [16,18–21]. The numerous experiments were performed at different conditions: subsonic and supersonic flow; wall step, long cavity ($l/d = 6.5$), and short cavity ($l/d = 3.3$); different pressures $P_{st} = 100$–700 torr; current from 5 to 20 A; both polarities; etc. Here, the data for the wall step in supersonic flow $M = 1.9$–2.0 are shown for typical parameters of electrical discharge. The data are compared with the results of CFD analysis.

The scheme of the test arrangement is shown in Fig. 29. The discharge insertion was mounted upstream of the fixed separation zone. Two different modes of the discharge operation have been found in the case of the separation zone. At the first mode, the discharge is excited between electrodes. At the second mode, the discharge current is being connected to the metallic wall in the

Table 3 Comparison of experimental data for different gases

Gas	Power, kW	Shock's shift, mm	Extrusive-layer thickness	$P_0 2$ change, %	$P_{st} 3$ change, %
Air	1.75	20	8	−8%	−3%
Argon	1.7	5	5	0	−2%
CO_2	1.8	10	4	+3%	+7%

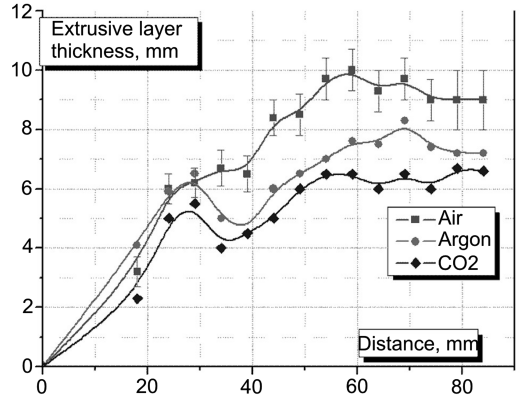

Fig. 28 Extrusive-layer thickness in dependence on the sort of gas.

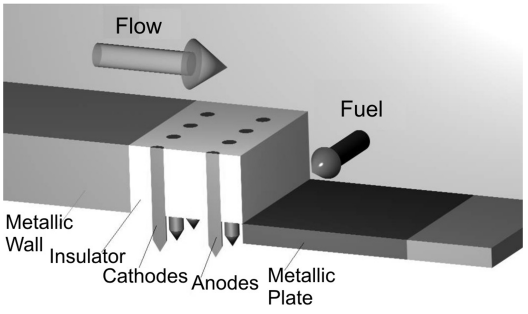

Fig. 29 Test arrangement in fixed separation zone.

separation zone. We are talking about the second mode as the most promising for an application [21]. Electric energy release in the plasma volume has the value of $W_{\rm pl} = 2$–10 kW at the transversal size of the plate of about 70 mm (facility PWT-50).

The discharge dynamics in flow behind the wall step and in cavity were explored using a high-speed digital complementary metal-oxide semiconductor (CMOS) camera with a typical frame rate of 2000 frames per second at 1280×250 pixels and exposure down to 10 μs. As a sample in Fig. 30, selected frames are presented for operation in supersonic mode behind the wall step and in the cavity for a comparison.

It is seen that in the case of the cavity, the discharge filaments look unstable. A full frame sequence shows a fast movement of them in the separation zone. An S type of plasma filaments shape reflects the flow velocity distribution under separation. An intensification of flow circulation due to energy release is also proved by simulation (discussed subsequently). In contrast, the shape of the discharge filaments is very stable in supersonic mode with a backwise wall step. The plasma filaments' location practically repeats the edge of separation. The power release weakly depends on static pressure under explored conditions ($M = 1.9$). The field's magnitude significantly higher than with the case of subsonic flow. Because of the field elevation ($E/n \approx 5 \times 10^{-16}$ Vcm^2), the electron temperature has to be increased as well from $T_e = 0.8$ to approximately 1.5 eV.

The method of optical spectroscopy is used to measure plasma temperature [20]. Measurements were carried out at three different values of ballast resistances (resulting in a variation of power and a reduced electrical field) in the separation zone of the duct. Temperature was measured by the fitting of experimental and calculated spectra of the N_2 second positive system (0-0, 337.1 nm) and of the violet system of cyan (CN) (388.9 nm). By the analysis of the N_2 spectra, the rotational temperature was the same for different conditions: its value is $T_r = 3.0$ kK $\pm$ 0.2 kK. Temperature measurements carried out by the CN spectrum give the following results: $T_v = 7.5$ kK $\pm$ 0.5 kK and $T_r = 7$ kK $\pm$ 0.5 kK. Such high values are explained by the fact that we measure the temperature of the excited state of the CN molecules, whereas rotational temperature measured by the N_2 spectrum is equal to the temperature of the N_2 ground state. It is clear that under conditions of high nonuniformity of the discharge structure, the measured magnitude of temperature poses between maximal and average values, closer to the first one. Therefore, the different molecular bands can give different formal temperatures. As an example of such measurement, the data for a molecular ion of nitrogen N_2+ were obtained as well. The formalized procedure of temperature recalculation gives $T_r = 9 \pm 3$ kK. Extra efforts are now being made to resolve such a discrepancy. The averaged gas temperature in the cavity is evaluated on the basis of heat balance at a value of $\Delta T_{\rm cav} \leq 200$ K.

As before, two methods were mainly used to study the discharge effect on the flow structure behind the wall step: pressure measurements and schlieren visualization. A 16-channel pressure recorder was used in the tests. The typical data are presented in Fig. 31. The sensor's position is indicated in the figure's inset.

The schlieren system was adjusted to work in pulse mode of the flash lamp with a frame frequency $f = 100$ Hz. The images in Fig. 32 are presented by a pair (discharge off/on) for the operation modes when the averaged power deposition is in the range of $W_{\rm av} = 5$–7 kW and static pressure $P_{\rm st} = 120$–180 torr in supersonic mode at $M \approx 1.9$. The exposure is about $t = 1$ μs. As can be recognized easily, the discharge effect on the flow structure lies in an

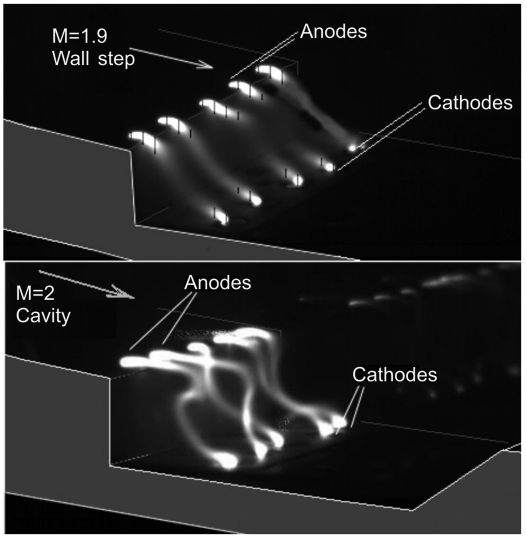

Fig. 30 Discharge appearance in supersonic mode behind backwise wall step and in cavity.

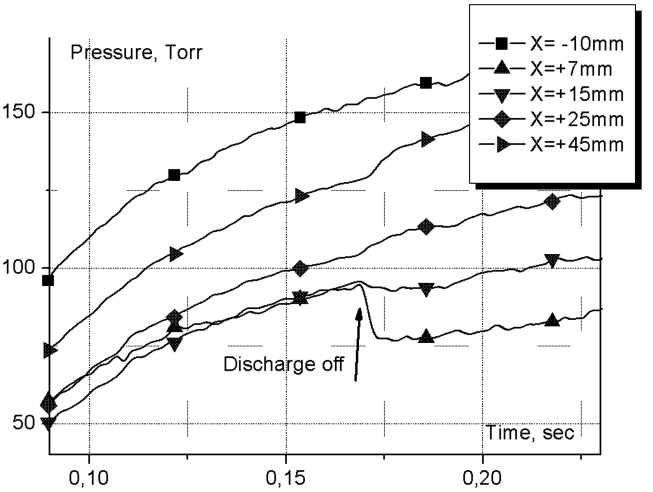

Fig. 31 Pressure record at $M = 1.9$ and $W_{\rm av} = 5.95$ kW; discharge is switched on before flow start and switched off in $t = 0.17$ s; and coordinate X is in respect to the step position.

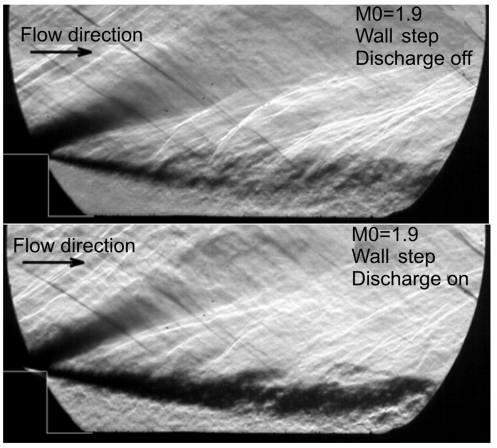

Fig. 32 Schlieren photographs of the discharge effect on flow structure; supersonic mode; wall step.

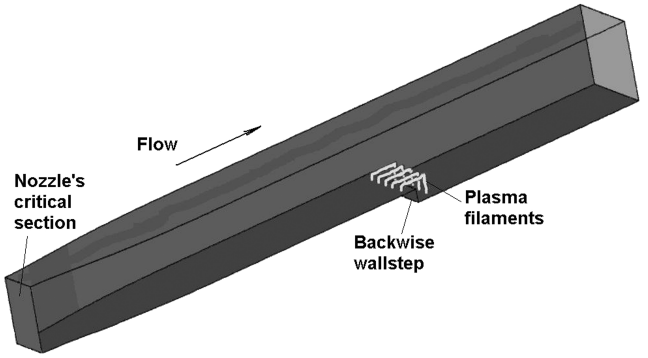

Fig. 33 Geometry of settlement area.

intensive turbulization (mixing) of gas in the interaction area at a simultaneous slight increase of the separation-zone volume.

Numerical modeling of flow in the experimental setup was based on the solution of 3-D time-dependent Reynolds-averaged Navier–Stokes equations with the use of the widely used two-equation supersonic transport (SST) model of turbulence. Calculation of three-dimensional turbulent flow in the frame of the model of perfect gas in the experimental setup was executed by modeling a heat supply caused by the direct-current electric discharge. The geometry of the whole channel and areas of thermal input in it are shown in Fig. 33. Constant values of velocity $V = 317$ m/s, total pressure $P_0 = 10^5$ Pa, and temperature $T = 250$ K were specified in the initial section of the calculation domain, which is the critical section of the $M = 2$ supersonic nozzle. Zero gradients of flow parameters in the outlet section of the calculation domain were fixed. No-slip and adiabatic conditions were specified on the upper and lower walls and one lateral wall of the duct as well as on the cavity walls. Symmetry conditions were used in the median section of the duct to decrease the calculation domain, which contained 600,000 mesh points.

Five heat sources shown in Fig. 33 with a constant density of thermal power deposition were specified. The cross sections of both vertical and horizontal parts of each heat source have the form of a square with a side of 3 mm. The middle of the forward vertical part of a source was placed at an upstream distance of 10 mm from a vertical wall of a cavity (step), and the middle of the back vertical part was at a distance of 20 mm from this wall downstream. The thermal power of each source was equal to 1 kW. Total heat input in the flow was equal to $W = 5$ kW. Heat-addition modeling takes into account the chemical-reaction phenomenon, which is critically important at high temperature. It is assumed that the air gas is a mixture of 5 components: O_2, O, N_2, N, and NO.

For the wall-step configuration without heat addition, a strong rarefaction wave accelerates flow to Mach number $M = 2.5$ (Fig. 34a), whereas at the heat supply, a shock wave arises ahead of a

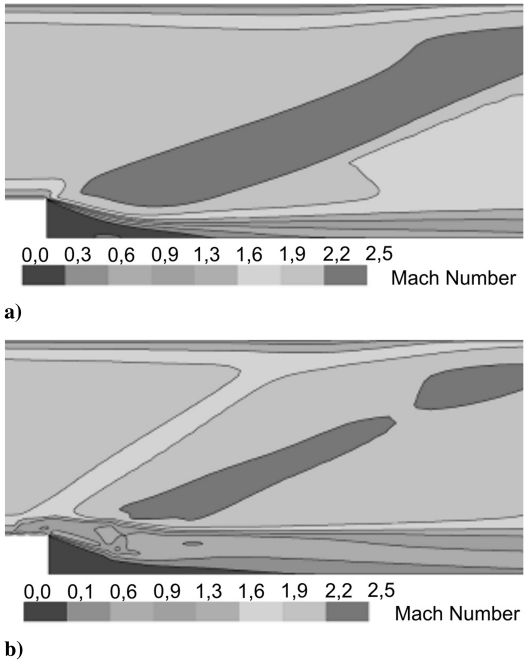

Fig. 34 Mach number distribution in a plane of symmetry for discharge a) off and b) on.

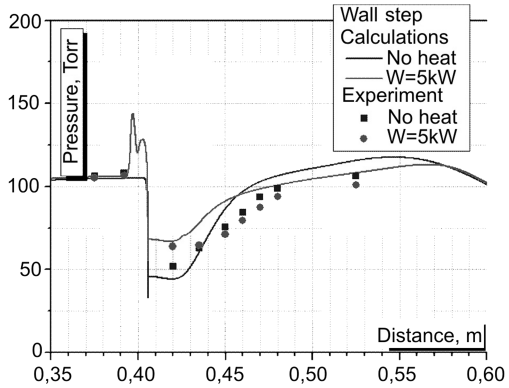

Fig. 35 Comparison of calculated and experimental pressure distribution behind the wall step in the supersonic duct.

thermal source, the mixture layer becomes notably thicker, and a weak rarefaction wave consequently accelerates flow to only $M = 2.3$ (Fig. 34b). The Mach number has a local minimum in the vicinity of the horizontal part of the thermal source. It is determined by an essential rise in temperature.

Figure 35 presents the comparison of calculated and experimental pressure distributions in the separation zone along the bottom wall. It can be seen that the trend is similar, with an insufficient difference in absolute values. Summarizing the discharge effect on the pressure distribution behind the wall step, it should be considered that, as a rule, the pressure rises noticeably near the discharge zone and its distribution occurs smoother as a whole.

The essentially three-dimensional character of the considered flow is demonstrated by CFD data. The important issue is a rate of gas exchange between the main flow and the separation zone. The calculated values are equal to $G_0 = 0.0054$ kg/s and $G_Q = 0.0074$ kg/s, respectively, without heat input and with it. The experimental value on the velocity of gas circulation in the separation zone gave a similar result.

V. Conclusions

The generation of surface-localized discharges in a high-speed flow makes possible the substantial change of the structure and

parameters of the flowfield. This paper examined several aspects of the problem: namely, peculiarities of the discharge excitation in the flow, the effect of discharge on the flow structure and parameters, the effect of screening of a mechanical obstacle, and control of flow parameters behind a backwise wall step and in the inlet's configuration. For a better understanding of the problem, a simplified interaction model was proposed, and the experimental findings were compared with the results of analytical prediction and numerical simulation.

The transversal electrical discharge in the flow basically changes its structure relative to the situation in motionless gas. Individual plasma filaments with a typical gas temperature of about 3 kK move with the flow downstream until they break in consequence of a voltage rise, with a subsequent breakdown in a new place. The frequency of such relaxations depends on the experimental parameters and was about 50 kHz or less in the case in point.

This discharge affects the flow in a manner similar to the effect on a soft wedge, for which the angle depends on the electrical power release. At exceeding the value of about $W/P_{st} \approx 10 \times z$ W/torr, where z is the discharge-region depth, the flow separates downstream with subsequent attachment or without it. The discharge generation is accompanied by the formation of an oblique shock, for which the amplitude allows regulation with the aid of electrical parameters. Accordingly, the main flow properties vary in a controllable way.

Excitation of the near-wall heated layer and artificial separation zone allows partial screening of the obstacle on the wall. Reduction of the obstacle drag in the flow may reach 95%. The energy efficiency of such screening depends on the shape of the obstacle. For a streamlined contour, this method is of little effect, whereas for a blunt body, the effectiveness may be of the order of magnitude. In this case, kinetic power losses in the channel markedly decline, which is reflected in a rise of the overall pressure recovery coefficient. The experiments fulfilled in different practically important geometrical configurations have demonstrated a significant benefit of the plasma technique in the shock's structure control and mixing intensification.

The principal regularities of the discharge interaction with a supersonic flow are adequately described by the proposed simplified model, including the position and angle of the oblique shock and the gas temperature in the heated layer. At the same time, failure to take into account processes of plasma-chemical transformations and respective loss of energy results in a somewhat higher value of the plasma wedge angle.

Acknowledgments

A part of the work was funded in 2001–2004 by European Office of Aerospace Research and Development (International Science and Technology Center project ISTC 2084p, John Schmisseur's supervision). In 2003–2005, the work was supported also by program 20 of the Presidium of the Russian Academy of Sciences (coordinator academician Gorimir Chernyi). The authors express their gratitude to Konstantin Savelkin of the Joint Institute for High Temperatures at the Russian Academy of Sciences for valuable assistance in experimental work, to Anatoly Yuriev of Mozhaisky Engineering Space Academy for consulting on practical aerodynamics, to Victor Soloviev of the Moscow Institute of Physics and Technology for analysis of vibrational–translational relaxation effects in high-speed flow, to Valery Gromov of the Institute of Mechanics at Moscow State University, and to Mikhail Starodubtsev of the Central Aerohydrodynamic Institute for numerous computational fluid dynamics efforts. The authors are thankful to Sergey Macheret for advice on the style of the paper.

References

[1] Leonov, S., Bityurin, V., "Hypersonic/Supersonic Flow Control by Electro-Discharge Plasma Application," AIAA Paper 2002-5209, Oct. 2002.

[2] Bletzinger, P., Ganguly, B. N., VanWie, D., Garscadden, A., "Plasmas in High Speed Aerodynamics," *Journal of Physics D: Applied Physics*, Vol. 38, Feb. 2005, pp. R33–R57. doi:10.1088/0022-3727/38/4/R01

[3] Leonov, S., Bityurin, V., Klimov, A., Kolesnichenko, Yu., Yuriev, A., "Influence of Structural Electric Discharges on Parameters of Streamlined Bodies in Airflow," AIAA Paper 2001-3057, June 2001.

[4] Fomin, V., Tretyakov, P., Taran, J.-P., "Flow Control Using Various Plasma and Aerodynamic Approaches," *Aerospace Science and Technology*, Vol. 8, Dec. 2004, pp. 411–421. doi:10.1016/j.ast.2004.01.005

[5] Macheret, S., Miles, R., Schneider, M., "Comparative Analysis of MHD and Plasma Methods of Scramjet Inlet Control," AIAA Paper 2003-0170, Jan. 2003.

[6] Leonov, S. B., Savelkin, K. V., Yarantsev, D. A., Gromov, V. G., "Aerodynamic Effects Due to Electrical Discharges Generated Inflow," *Proceedings of the European Conference for Aerospace Sciences* [CD-ROM], European Conference for Aerospace SciencesJuly 2005.

[7] Leonov, S., Kuriachy, A., Yarantsev, D., Yuriev, A., "Mechanisms of Flow Control by Near-Surface Electrical Discharge," AIAA Paper 2005-0780, Jan. 2005.

[8] Leonov, S. B., Yarantsev, D. A., Isaenkov, Yu. I., "Properties of Filamentary Electrical Discharge in High-Enthalpy Flow," AIAA Paper 2005-0159, Jan. 2005.

[9] Leonov, S. B., Yarantsev, D. A., Gromov, V. G., Isaenkov, Yu. I., Soloviev, V. R., "The Gas-Dynamic Phenomena Associated with Surface Discharge in High-Speed Flow," *Proceedings of the 15th International Conference on MHD and MPA*, Vol. 3, Joint Inst. for High Temperature, Russian Academy of Sciences, Moscow, 24–27 May 2005, pp. 758–768.

[10] Leonov, S., Bityurin, V., Bocharov, A., Gubanov, E., Kolesnichenko, Yu., Savelkin, K., Yuriev, A., Savischenko. N., "Discharge Plasma Influence on Flow Characteristics Near Wall Step in a High-Speed Duct," *Proceedings of the 3rd Workshop on Magneto-Plasma Aerodynamics in Aerospace Applications*, Joint Inst. for High Temperature, Russian Academy of Sciences, Moscow, 24–26 Apr. 2001, pp. 58–66.

[11] Leonov, S. B., Kuriachii, A. P., Yu, I., Soloviev, V. R., Yarantsev, D. A., "Supersonic/Transonic Flow Control by Electro-Discharge Plasma Technique," International Congress on Aeronautical Science Paper 409, Sept. 2006.

[12] Bityurin, V., Gromov, V., Leonov, S., Savischenko, N., Yuriev, A., "Influence of Surface Electrical Discharge on Friction of Plate in Subsonic and Transonic Airflow," AIAA Paper 2001-0640, Jan. 2001.

[13] Abramovich, G. N., *Applied Gas Dynamics*, Nauka, Moscow, 1976, p. 888.

[14] Macheret, S. O., Shneider, M. N., Miles, R. B., "Magneto-hydrodynamic Control of Hypersonic Flows and Scramjet Inlets Using Electron Beam Ionization," *AIAA Journal*, Vol. 40, No. 1, Jan. 2002, pp. 74–81.

[15] Leonov, S., Soloviev, V., Yarantsev, D., "44th High-Speed Inlet Customization by Surface Electrical Discharge," AIAA Paper 2006-0403, Jan. 2006.

[16] Leonov, S., Bityurin, V., Yarantsev, D., "The Effect of Plasma-Induced Separation," AIAA Paper 2003-3853, June 2003.

[17] Leonov, S., Nebolsin, V., Shilov, V., "Effectiveness of Plasma Jet Effect on Bodies in an Airflow," *Perspectives of MHD and Plasma Technologies in Aerospace Applications*, Inst. for High Temperature, Russian Academy of Sciences, Moscow, 1999, pp. 58–65.

[18] Leonov, S., Yarantsev, D., Kuryachii, A., Yuriev, A., "Study of Friction and Separation Control by Surface Plasma," AIAA Paper 2004-0512, Jan. 2004.

[19] Leonov, S. B., Yarantsev, D. A., Napartovich, A. P., Kochetov, I. V., "Plasma-Assisted Combustion of Gaseous Fuel in Supersonic Duct," *IEEE Transactions on Plasma Science*, Vol. 34, No. 6, Dec. 2006, pp. 2514–2525. doi:10.1109/TPS.2006.886089

[20] Yarantsev, D. A., Leonov, S. B., Biturin, V. A., Savelkin, K. V., "Spectroscopic Diagnostics of Plasma-Assisted Combustion in High-Speed Flow," AIAA Paper 2005-3396, May 2005.

[21] Leonov, S. B., and Yarantsev, D. A., "Plasma-Induced Ignition and Plasma-Assisted Combustion in High-Speed Flow," *Plasma Sources Science and Technology* , Vol. 16, Feb. 2007, pp. 132–138. doi:10.1088/0963-0252/16/1/018

S. Macheret
Associate Editor